PLOS | ONE

RESEARCH ARTICLE

Growth and Potential Damage of Human Bone-Derived Cells Cultured on Fresh and Aged C_{60}/Ti Films

Ivana Kopova[1]*, Vasily Lavrentiev[2], Jiri Vacik[2], Lucie Bacakova[1]

1 Institute of Physiology, Czech Academy of Sciences, Videnska 1083, 142 20, Prague, 4—Krc, Czech Republic, **2** Nuclear Physics Institute, Czech Academy of Sciences, 250 68, Rez near Prague, Czech Republic

* ivana.kopova@biomed.cas.cz

Citation: Kopova I, Lavrentiev V, Vacik J, Bacakova L (2015) Growth and Potential Damage of Human Bone-Derived Cells Cultured on Fresh and Aged C_{60}/Ti Films. PLoS ONE 10(4): e0123680. doi:10.1371/journal.pone.0123680

Academic Editor: Juha Tuukkanen, University of Oulu, FINLAND

Received: May 2, 2014

Accepted: March 6, 2015

Published: April 15, 2015

Data Availability Statement: Tha data underlying our findings is available either freely in the manuscript in the form of pictures (qualitative data) or in the form of Mean ± S.E.M. The data from which these values was calculated is available upon request.

Funding: This research was supported by the Grant Agency of the Czech Republic (grants No. P107/11/1856 and P108/12/1168) and CANAM infrastructure (NPI ASCR Rez).

Competing Interests: The authors have declared that no competing interests exist.

Abstract

Thin films of binary C_{60}/Ti composites, with various concentrations of Ti ranging from ~ 25% to ~ 70%, were deposited on microscopic glass coverslips and were tested for their potential use in bone tissue engineering as substrates for the adhesion and growth of bone cells. The novelty of this approach lies in the combination of Ti atoms (i.e., widely used biocompatible material for the construction of stomatological and orthopedic implants) with atoms of fullerene C_{60}, which can act as very efficient radical scavengers. However, fullerenes and their derivatives are able to generate harmful reactive oxygen species and to have cytotoxic effects. In order to stabilize C_{60} molecules and to prevent their possible cytotoxic effects, deposition in the compact form of Ti/C_{60} composites (with various Ti concentrations) was chosen. The reactivity of C_{60}/Ti composites may change in time due to the physicochemical changes of molecules in an air atmosphere. In this study, we therefore tested the dependence between the age of C_{60}/Ti films (from one week to one year) and the adhesion, morphology, proliferation, viability, metabolic activity and potential DNA damage to human osteosarcoma cells (lines MG-63 and U-2 OS). After 7 days of cultivation, we did not observe any negative influence of fresh or aged C_{60}/Ti layers on cell behavior, including the DNA damage response. The presence of Ti atoms resulted in improved properties of the C_{60} layers, which became more suitable for cell cultivation.

Introduction

Fullerenes are spheroidal hollow cage-like carbon nanoparticles with diverse biological activities. Due to their unique physicochemical properties, e.g. the ability to withstand high temperatures and pressures, and also the high reactivity of these nanoparticles, fullerenes are expected to have great potential in a wide range of fields including medicine. The high reactivity of these molecules has been explained by bending of sp^2-hybridized carbon atoms, which produces angle strain, and by the presence of double bonds, which can react with radical species. Fullerenes C_{60} and their derivatives are therefore considered to be the world's most efficient radical

scavengers with strong antioxidant properties (for a review, see [1, 2]). For example, fullerene C_{60} and its derivative fullerol has been reported to antagonize the oxidative stress generated by dexamethasone therapy, and thus to prevent osteonecrosis [3, 4]. By quenching oxygen radicals, fullerenes C_{60} also inhibit the differentiation of osteoclasts and the production of matrix metalloproteases, and can thus inhibit the destruction of bone and cartilage tissue in arthritis [5, 6]. Complexes of fullerenes with polyvinylpyrrolidone (with fullerene C_{60} as the major component) displayed photoprotective effects on keratinocytes against ultraviolet B irradiation [7].

However, fullerenes are able not only to quench, but also to generate dangerous reactive oxygen species (ROS). Numerous studies have described fullerenes as a cytotoxic and genotoxic agent, causing oxidative DNA damage [8, 9], inhibition of detoxificatory and antioxidant enzymes [10], polyploidy [11], premature cell senescence [12], apoptosis [13] and inflammation [14]. The biological response to fullerenes is profoundly influenced by their physical and chemical properties, such as water solubility [15]; for a review, see [16], functionalization with various chemical groups [17], electronic behavior, degree of agglomeration [13], and also concentration [14]. For example, increased water solubility was associated with decreased cytotoxicity of C_{60}. On the other hand, certain solvents can enhance fullerene toxicity (for a review, see [16]). The carboxylate derivatization of fullerenes was the determining factor in their ability to induce apoptosis in human monocytic THP1 cells [13]. At lower concentrations (less than 0.04mg/ml), fullerene-based amino acid nanoparticles 0.04 mg/mL initiated less cytokine activity and maintained the viability of human keratinocytes, while at higher concentrations (0.04 to 0.4 mg/ml) these nanoparticles were cytotoxic and pro-inflammatory [14].

In order to prevent possible cytotoxic effects of fullerenes, deposition of these molecules in the form of compact and stable layers, well-adhering to the underlying substrate, was chosen. We supposed that the fullerene films could be strengthened by introducing a biocompatible metallic component into the films. Fullerene C_{60}-gold nanoparticle films, self-assembled on silanized glass coverslips, showed good chemical and ultrasonic stability, as revealed by their immersion in 0.1 M HCl and by their exposure to ultrasonic irradiated surrounding [18]. The introduction of a suitable metallic component was expected to stabilize the fullerene films in terms of reducing the release of free C_{60}, their penetration into cells, and thus to eliminate the potential negative effects of fullerenes. Titanium was chosen as this metallic component, due its biocompatibility, which has been proven in its numerous and long-lasting experimental and clinical applications. Titanium is a metal that has been widely used for constructing stomatological implants and, in the form of alloys, such as Ti-6Al-4V or newly developed beta-titanium alloys, also for orthopedic implants, such as load-bearing joint replacements [19–22]; for a review, see [23]. Titanium was also tested with positive results in our earlier studies as a potential component of carbon-based coatings of bone implants, namely amorphous carbon with titanium [24] or hydrocarbon plasma polymers enriched with Ti [25]. Specifically, the presence of Ti in these coatings enhanced the adhesion, spreading, growth and production of osteocalcin in human osteoblast-like MG-63 cells. The presence of Ti in diamond-like carbon (DLC) coatings also increased their bioactivity compared to pure DLC. This was manifested by precipitation of compounds containing calcium and phosphorus, i.e., basic components of the bone apatite, and by increased colonization of Ti-doped DLC with human osteoblast-like MG 63 cells [26]. At the same time, the addition of Ti into DLC coatings improved their mechanical properties, namely by increasing their adhesion to the underlying substrates [27], by decreased their residual stress and friction coefficient, and by modulating their hardness to appropriate values [28, 29].

The construction of C_{60}/Ti composites in this study was also inspired by our earlier studies and by studies by other authors, in which C_{60} was combined with transitional metals, namely Ni, Fe, Nb, Pt and Pd [30–34]. These composites showed interesting structural, electrotransport,

electrochemical and photoelectric properties, and are applicable in electronics or photovoltaics [35]; for a review, see [33]. However, with the exception of Nb, which is considered as biocompatible, all metals mentioned here are known to be cytotoxic. To the best of our knowledge, C_{60}/Ti composite films, with the exception of our earlier studies [36, 37], have not yet been constructed and investigated for biomedical purposes by other authors. In our earlier studies, only the adhesion and growth of MG-63 cells, measured by changes in their number in three time intervals, were investigated on C_{60}/Ti composite films, together with regional selectivity of cell colonization, if these films were constructed as micropatterned, i.e. containing grooves and prominences [36, 37]. The novelty of present study lies in the deeper investigation of the cell behavior on C_{60}/Ti films, including not only their adhesion and growth, but also their viability, mitochondrial activity, and potential DNA damage.

Another important factor investigated in our study is the influence of the age of C_{60}/Ti composites on these parameters, as well as on the regional selectivity of the cell colonization on films with a micropatterned morphology. In our earlier study performed on pure fullerene C_{60} films, fresh fullerene films lowered the cell number, viability, growth and metabolic activity, and these parameters improved markedly with aging of the C_{60} films [38]. Moreover, micropatterned fresh fullerene films promoted regionally-selective cell colonization in grooves among the prominences, which almost disappeared on aged fullerene films. These results were attributed to changes in the fullerene films during aging, e.g. fragmentation, oxidation, polymerization and graphitization of fullerenes in an air atmosphere, and thus loss of their reactivity [38].

Last but not least, the C_{60}/Ti fullerene films in the present study were deposited with three different concentrations of Ti, ranging from ~ 25% (i.e., 25 Ti atoms and 75 C_{60} molecules) to ~ 70%, in order to investigate potential differences in their stability and in the cell behavior on these surfaces. On DLC films doped with three concentration levels of Ti (up to 23 at. %), the number of MG-63 cells increased with the increasing Ti concentration. They were highest on DLC with a medium and highest content of Ti [26].

Material and Methods

Material deposition

The C_{60}/Ti composite films were prepared by co-deposition of C_{60} and Ti onto microscopic glass coverslips (Menzel-Gläser, Germany, diameter 12 mm) in the Molecular Beam Epitaxy (MBE) chamber using the Knudsen cell and an e—gun for vaporization of C_{60} and Ti, respectively (**Fig 1**), under certain deposition kinetics: background pressure during deposition ~ 5×10^{-7} Torr; deposition rate ~ 1 nm/min; temperature of the substrates during deposition ~ room temperature (RT). Three C_{60}/Ti systems, with different phase ratios, were fabricated, i.e., with a low concentration (25%, i.e., 25 Ti atoms and 75 C_{60} molecules), medium concentration (45%) and high concentration (70%) of Ti atoms in the composite.

The composites were synthesized with a micropatterned morphology by deposition through a contact mask (a metallic mesh) producing rectangular C_{60}/Ti prominences with an average size of 128 μm per 98 μm (12,500 μm^2) and with 50 μm spacing. However, as revealed by Raman spectroscopy and AFM, these spaces (grooves) also contained a very thin continuous film of C_{60}/Ti composites.

The samples were stored for 1–2 weeks (fresh samples) or for 1 year (aged samples) in an air atmosphere at room temperature in a dark and dry place, and were then evaluated.

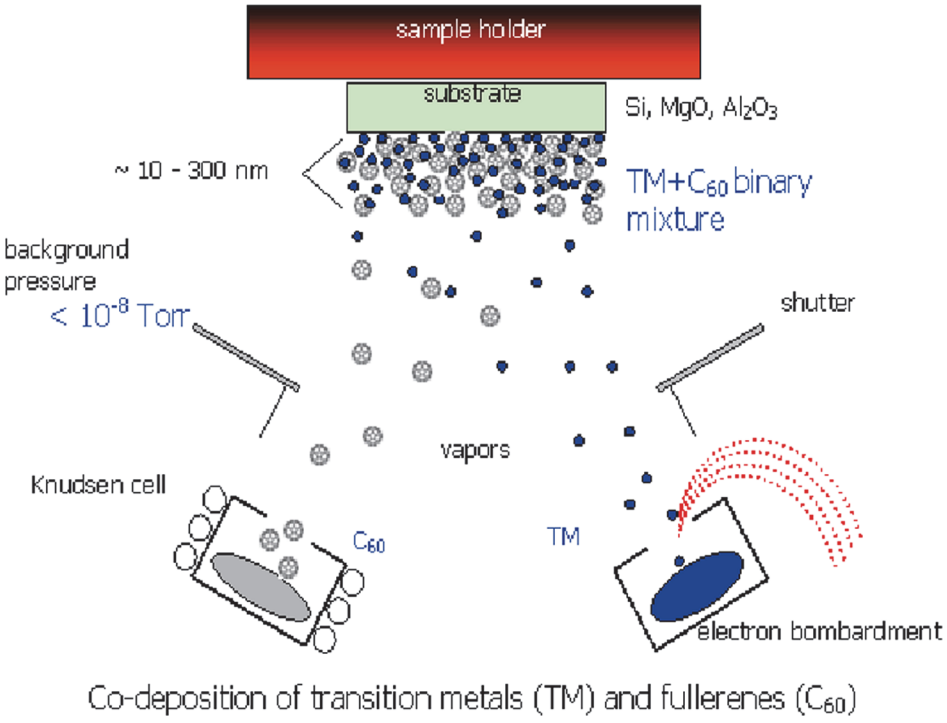

Fig 1. Scheme of the preparation of hybrid fullerene C_{60}/metal composites. Deposition rates: DR(M) = DR(C_{60}) ~ 1 nm/min. Temperatures during deposition: RT.

doi:10.1371/journal.pone.0123680.g001

Raman spectroscopy

A Renishaw 2000 imaging microscope (using a 514 nm Ar laser) was applied for an analysis of the C_{60}/Ti films. The measurements were performed using low laser power, i.e., (< 1 mW) in order to avoid fragmentation of the C_{60} molecules. The spectra were measured on the top of the C_{60}/Ti prominences, using multi-peak Gaussian analysis of the $H_g(7)$, $A_g(2)$ and $H_g(8)$ vibration peaks. Area peak ratios $A_g(2)/H_g(7)$ and $A_g(2)/H_g(8)$ were evaluated.

Atomic force microscopy (AFM)

The surface morphologies of the C_{60}/Ti layers were analyzed by atomic force microscopy (AFM microscope NTEGRA, NT-MDT) using a static (contact) mode. The scanning area was selected as 5 x 5 μm^2.

Stability of C_{60}/Ti coating (potential water dissolution)

All examined C_{60}/Ti coatings with a low, medium and high content of Ti were incubated in 1 ml of deionized water at 37°C in a humidified air atmosphere containing 5% of CO_2 for 24 hours (mimicking the rinsing phase prior to use for all biological experiments; described below in Cells and culture conditions). After 24 hours, the water was transferred from the C_{60}/Ti samples to glass Petri dishes (diameter 2 cm), and fresh deionized water was added to the same C_{60}/Ti samples for further 48 hour-long incubation (mimicking the incubation phase with cells in biological experiments). The water solutions were slowly dried on glass Petri dishes for 2 days. When all water was evaporated, the thin films that had formed on the bottom of the Petri dishes were analyzed by Raman spectroscopy.

Measurement of wettability

The surface wettability of the C_{60}/Ti composites was estimated from the contact angle measured by a material-water droplet system using a reflection goniometer (SEE System, Masaryk University, Brno, Czech Republic). The data was presented as mean ± standard error of the mean (S.E.M.) obtained from 10 measurements.

Cells and culture conditions

Since the samples were prepared under aseptic conditions (assured by the high temperature), sterilization was not performed in order to avoid potential damage to the fullerene molecules by irradiation, heating or chemicals. However, to prevent the potential release of newly deposited C_{60}/Ti molecules into the culture medium, all samples (i.e., glass coverslips coated with C_{60}/Ti films with various Ti concentrations) were incubated in deionized water at 37°C in a humidified air atmosphere containing 5% of CO_2 for 24 hours prior to each biological experiment. The samples were then repeatedly rinsed in phosphate-buffered saline (PBS; Sigma, Missouri, U.S.A.). For studies on cell adhesion, spreading, growth, morphology, viability and metabolic activity, the samples were seeded with human osteoblast-like MG-63 cells (European Collection of Cell Cultures, UK) in an initial density of 5 370 cells/cm^2 (10 000 cells per well). For studies on DNA damage, human osteoblast-like U-2 OS cells (ATCC-LGC, No. HTB-96) were used in densities ranging from 4 300 cells/cm^2 (8 000 cells per well) to 16 100 cells/cm^2 (30 000 cells per well). Both cell lines were cultured for 1, 3 or 7 days in 1 mL of Dulbecco's Modified Eagle's Medium (Sigma, Missouri, U.S.A., Cat. No. D5648) supplemented with 10% fetal bovine serum (Sebak GmbH, Germany) and gentamicin (40 μg/mL; LEK, Slovenia) at 37°C in a humidified air atmosphere containing 5% of CO_2. Uncoated microscopic glass coverslips (Menzel-Gläser, Germany; diameter 12 mm) were used as a reference material. For each experimental group and time interval, 3 samples were analyzed, and the experiment was repeated three times.

Evaluation of cell morphology, initial adhesion and proliferation

The MG-63 cells were cultured for 7 days (seeding density 5 370 cells/cm^2; 10 000 cells per well). An evaluation of the cell morphology was performed on days 1, 3 and 7 after seeding, using an IX-71 microscope equipped with a DP-71 digital camera (Olympus, Japan). Immediately after that, each sample was transferred to fresh polystyrene 24-well tissue culture plates and rinsed with PBS. The cells were detached by a trypsin-EDTA solution (Sigma, Missouri, U.S.A., Cat. No T4174) and were counted using a Bürker haemocytometer (days 1 and 3) or using a Vi-Cell XR analyzer on day 7 (Beckman Coulter, California, U.S.A.). The cell numbers were expressed as cell population densities/cm^2 and were also used for calculating the cell population doubling time according to the following formula:

$$DT = \log 2 \frac{t - t_0}{\log N_t - \log N_{t_0}}$$

where t_0 and t represent earlier and later time intervals after seeding, respectively, and N_{t0} and N_t are the numbers of cells at these intervals.

In order to confirm the validity of the results, the experiments were repeated and data from separate experiments was analyzed. For each experimental group and time interval, three parallel samples were evaluated, and the experiment was repeated three times.

Evaluation of cell metabolic activity

The commercial Cell Proliferation Kit II XTT (Roche, Switzerland, Cat.No.11 465 015 001) was used to investigate the potential cytotoxicity of the C_{60}/Ti films. This is a set of colorimetric assays based on cleavage of the yellow tetrazolium salt XTT (2,3-bis(2-methoxy-4-nitro-5-sulphophenyl)-2H-tetrazolium-5-carboxanilide) to a soluble orange formazane derivate by mitochondrial enzymes from metabolically active cells (an indirect measure of the cell proliferation activity). The formazane dye is directly quantified by a spectrophotometer. After 3 and 7 days of cultivation, all samples were transferred to new polystyrene 24-well tissue culture plates and were rinsed with PBS. A 1 mL solution of XTT and Dulbecco's Modified Eagle's Medium without Phenol Red (Gibco, Cat. No 11053–028), supplemented with 10% fetal bovine serum (Sebak GmbH, Germany) and gentamicin (40 μg/mL; LEK, Slovenia) in the ratio of 1 volume part of XTT to 2 volume parts of DMEM, was added to each sample (according to the manufacturer's protocol). After 4–6 hours of incubation at 37°C in a humidified air atmosphere containing 5% of CO_2, the absorbance of the resulting solution was measured at wavelength 470 nm against the reference value of 650 nm.

Solutions from C_{60}/Ti-coated samples and also from uncoated microscopic glass coverslips without seeded cells were used as blank samples. In order to confirm the validity of the results, the experiment was repeated three times, and the data from separate experiments was analyzed. For each experimental group and time interval within one experiment, three parallel samples were used and the solution from each well was divided into 8 parallel wells.

Evaluation of membrane damage and cell viability

On day 7 after seeding, cell viability and membrane damage to cells were detected by trypan blue staining performed during cell counting in the Vi-CELL XR analyzer (Beckman Coulter, California, U.S.A.). Data from three separate experiments was analyzed. For each experimental group, 50 images from three parallel samples were evaluated within one experiment.

Evaluation of the DNA damage response

In order to investigate potential DNA damage to the cells, osteosarcoma cell line U-2 OS was used instead of MG-63, which is p53 deficient. After 3 and 7 days of cultivation, the DNA damage response was evaluated by immunofluorescence staining analyzed by fluorescence microscopy and flow cytometry.

The samples for microscopy were rinsed with PBS and fixed with 4% paraformaldehyde (PFA; Sigma, Missouri, U.S.A.) for 20 minutes at room temperature. Subsequently, the cells were permeabilized with 0.1% Triton X-100 in PBS (Sigma, Missouri, U.S.A.) for 20 minutes at room temperature. This solution also contained 1% bovine serum albumin for blocking non-specific binding sites for antibodies. The samples were incubated with primary antibodies anti-53BP1 (0.2 μg/mL; Santa Cruz Biotech, California, U.S.A.; clone H-300) and anti-H2A.X-Phosphorylated Ser139 (0.4 μg/mL; Millipore, Massachusetts, U.S.A.; clone JBW301) for 1 hour, followed by secondary antibodies coupled to Alexa Fluor 488 and 546 (4 μg/mL; Invitrogen, Molecular Probes, Oregon, U.S.A.) for 1 hour. The cells were then mounted with a microscopic glass coverslip using a Gel/Mount permanent fluorescence-preserving aqueous mounting medium (Biomeda Corporation, California, U.S.A.) and were evaluated under the IX-71 epifluorescence microscope (Olympus, Japan) equipped with a DP-71 digital camera (Olympus, Japan).

The samples analyzed by flow cytometry were prepared using the same protocol as those for microscopy, except that all steps were performed in a suspension, not on microscopic glass coverslips. Alexa Fluor 488 anti-H2A.X-Phosphorylated (Ser139) antibody (5 μg/1 million cells; BioLegend, California, U.S.A.; clone 2F3) was used for flow cytometry. After 1 hour of incubation

with antibody, the cells were rinsed and resuspended in PBS. The samples were analyzed using an Accuri C6 Flow Cytometer (BD Biosciences, New Jersey, U.S.A.).

U-2 OS treated with neocarzinostatin (NCS; 700 ng/mL; Sigma, Missouri, U.S.A.) for 1 hour were used as a positive control to markers of a DNA damage response. The cells were fixed 3 hours after treatment with NCS. Immunofluorescence staining and also flow cytometry analysis were repeated in order to confirm the results.

Statistical analysis

The data was presented as mean ± S.E.M. (Standard Error of the Mean) or median with interquartile range (IQR) obtained from three separate experiments. Within each experiment, three samples for each experimental group and time interval were evaluated. A comparison between all groups was analyzed by two-way ANOVA, Student-Newman-Keuls Method, to evaluate two factors: the composition of the C_{60}/Ti layers (Ti content—25%, 45%, 70%) and their age (1 week or 1 year). *P*-values less than 0.05 were considered statistically significant.

Results and Discussion

Raman spectroscopy

A study by Raman spectroscopy measured on the top of the prominences revealed a change in both the fresh and aged fullerene films, in comparison with the C_{60} standard. **Fig 2A** depicts the Raman spectra (only relevant details between 1100–1800 cm^{-1}) measured on the fresh (i.e., 1-week-old) C_{60}/Ti composites deposited on glass coverslips at RT with a low (25%), medium (45%) and high (70%) concentration of Ti. For comparison, a Raman spectrum from the C_{60} standard (a film of C_{60} deposited on glass coverslips) is also shown. The main Raman vibration modes for fullerenes: $A_g(2)$, $H_g(7)$ and $H_g(8)$ were inspected. For all fresh layers, a change in the spectra revealed that the intensity of the most important $A_g(2)$ peak (pentagonal pinch mode, characteristic for fullerenes) dropped dramatically down (compared to the neighboring $H_g(7)$ and $H_g(8)$ vibration modes). Moreover, the $A_g(2)$ peak exhibits a significant red shift towards position 1450 cm^{-1}. The $H_g(7)$ and $H_g(8)$ modes remained on the same positions, but the area ratios $H_g(7)/A_g(2)$ and $H_g(8)/A_g(2)$ altered in comparison with the C_{60} standard. These changes are ascribed to alterations in the chemical bonding of C_{60}, such as polymerization (interaction of fullerene molecules into a polymerized network) and oxidation (chemical bonding of oxygen with fullerene molecules) [39]. It is known that $A_g(2)$ is the most sensitive vibration mode—by analyzing this mode one can get information about the C_{60} structural and bonding change (high sensitivity of Ti/C_{60} towards oxidation is described e.g. in [30]). All these changes are more obvious with increasing Ti content. In addition, new vibration modes G appeared in layers with a low and medium Ti content, indicating the formation of graphitic flakes.

An examination of aged (i.e., 1-year-old) C_{60}/Ti composites revealed dramatic difference in comparison with the fresh samples. The most important $A_g(2)$ mode is suppressed for all Ti concentrations, and $H_g(8)$ and G (formation of graphitic flakes and fragmentation of fullerenes) became the most prominent peaks. Another important difference of aged layers is the formation of the D band in films with low and medium Ti content, indicating disordered nanocarbon with sp^3 bonding (**Fig 2B**).

Degradation and oxidation of C_{60} films during aging was also proven by X-ray Photoelectron Spectroscopy (XPS) in our earlier study [38]. Alterations and fragmentation of fullerenes are enhanced in hybrid systems (transition metal/C_{60}) because of the strong catalytic properties of transition metals (including Ti) during co-deposition, which may cause the fullerene decay. The effect of aging was therefore least obvious in the samples with a high Ti concentration.

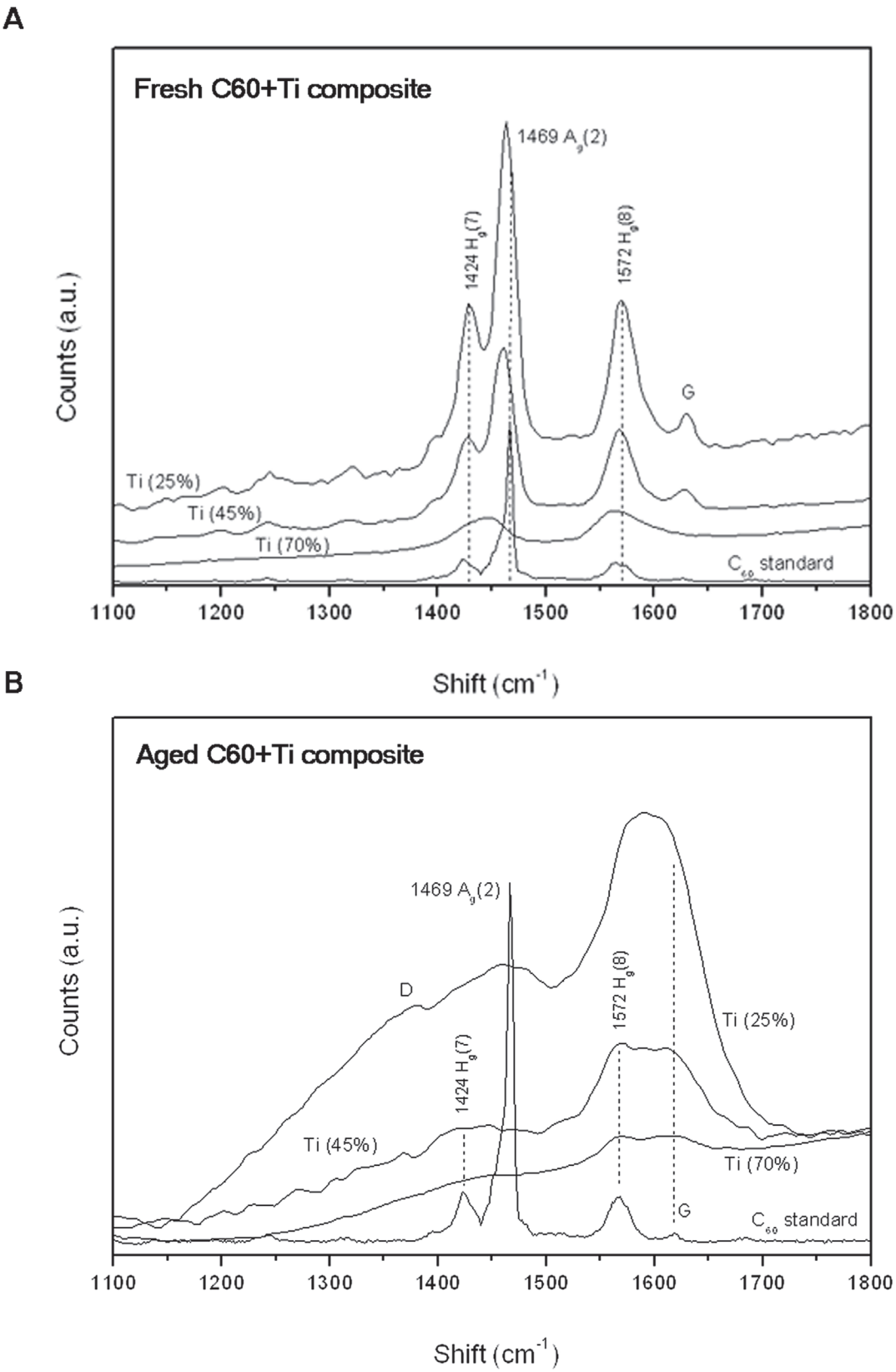

Fig 2. Raman spectra (between 1100–1800 cm^{-1}) of the fresh *(A)* and aged *(B)* C_{60}/Ti composites with various Ti concentrations (low: 25%, medium: 45%, high: 70%). For comparison, a spectrum from the C_{60} standard is shown.

doi:10.1371/journal.pone.0123680.g002

Based on reports from a similar system (with the combination of immiscible phases, i.e., C_{60}/Ni), the transition metal–fullerene hybrid composites, deposited at RT, are structurally stressed and exhibit a tendency toward phase separation [31, 32]. The final structure depends on the ratio of the building blocks (Ti and C_{60}), the thickness of the film and the temperature of preparation. Obviously, the different structure with different chemical bonds and surface morphology can have a different effect on the adhesion and growth of cells in biological systems.

Atomic force microscopy (AFM)

The morphology of the C_{60}/Ti films was analyzed by AFM (Fig 3) in the 5 x 5 μm^2 scanning areas. The thickness of the films varied from 10 nm (in grooves among the prominences) to about 300 nm (on the tops of the prominences). The ratio between the thicknesses of the C_{60}/Ti films at the prominences and in the grooves changed in the course of time, i.e., the ratio became lower in the aged composites (Table 1). This could be explained by a decrease in the height of the prominences after diffusion of the fullerenes, which was also observed in our earlier studies performed on pure micropatterned C_{60} films [38, 40].

In addition, the AFM images from the top of the prominences of all deposited systems with low (25%), medium (45%) and high (70%) atomic concentrations of Ti exhibited an interesting feature—the formation of particles with a different size (*S*) and area density (*D*), see Table 1. These particles, grown on the surface of the samples, were inspected by Raman spectroscopy and it was confirmed that they are large fullerene clusters with a low concentration of the Ti phase (causing only a mild disruption of the $A_g(2)$ pinch mode). This interesting effect was

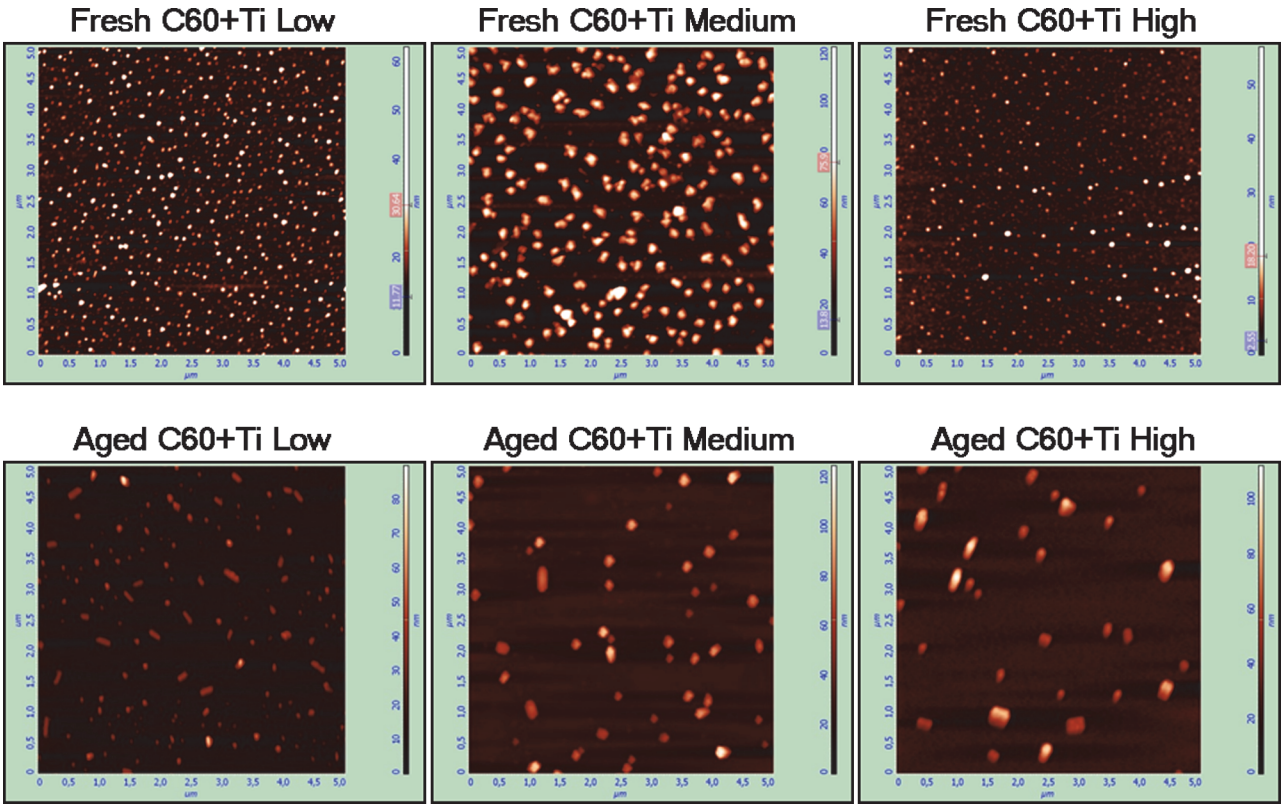

Fig 3. AFM images of the surface morphology on the prominences of the fresh and aged C_{60}/Ti composites with various Ti concentrations (low: 25%, medium: 45%, high: 70%).

doi:10.1371/journal.pone.0123680.g003

Table 1.

Parameter	Fresh C_{60}/Ti films	Aged C_{60}/Ti films
TP_{25} / TG_{25}	~ 8.3	~ 3.5
S_{25} [nm]	50–100	50–200
D_{25} [particles / 25 μm^2]	~ 650	~ 150
TP_{45} / TG_{45}	~ 10	~ 5.3
S_{45} [nm]	100–200	50–200
D_{45} [particles / 25 μm^2]	~ 250	50
TP_{70} / TG_{70}	~ 11.6	~ 4
S_{70} [nm]	25–75	50–150
D_{70} [particles / 25 μm^2]	~ 250	30

Main characteristics of the surface morphology of the prominences for fresh and aged (1-year-old) C_{60}/Ti thin films with various Ti concentrations (low: 25%, medium: 45%, high: 70%). TP/TG—ratio between the thickness of the prominences and the thickness of the grooves, S—particle size, D—particle area density. Scanning areas: 5 x 5 μm^2.

doi:10.1371/journal.pone.0123680.t001

already observed for the C_{60}/Ni hybrid system that was also prepared at RT [34]. The C_{60}/Ni composite was grown as a stressed, supersaturated mixture of two immiscible phases showing a strong proclivity to phase separation and particle network formation. After a year, about 200 particles per mm^{-2} several micrometers in size were formed. Interestingly, in the case of the C_{60}/Ti composites, all the observed particles had become smaller in size, the largest being only about 200 nm. The reason might be a limited reservoir (from a single prominence) for the diffusing fullerene molecules (building blocks for the grown particles), or different stress intensity (in comparison to the C_{60}/Ni system). On the other hand, the size of the C_{60}/Ti particles was larger than the typical granule size observed on pure C_{60} layers (~50 nm) [38]. In both (fresh and aged) cases, however, the morphology of the prominences changed, and this new nonostructural surface may be expected also to affect the biocompatibility of the hybrid system.

In addition, a different density of these clusters was observed on fresh and aged C_{60}/Ti layers. The number of C_{60}/Ti particles was higher on the fresh layers than on the aged films, but the size of the particles was slightly higher in the aged films (**Fig 3**, **Table 1**). This could be explained by fragmentation and diffusion of the fullerene molecules, and also by their polymerization and other changes in the C_{60}/Ti systems during the aging period.

Stability of C_{60}/Ti coating in a water environment

The stability of fresh C_{60}/Ti layers with a low, medium and high content of Ti was evaluated by dissolution in deionized water, and was analyzed by Raman spectroscopy. In the original (as deposited) films, the Raman measurements point to the dominant $A_g(2)$ breathing mode, confirming the presence of fullerenes (**Fig 2**; described above). However, the examination of the dried water in the Petri dishes, taken from the C_{60}/Ti films, did not prove any presence of fullerenes or other carbon allotropes. The Raman spectra showed only a broad luminescence distribution with Si-O-Si and O-H peaks from glass (Petri dish) and H_2O (**Fig 4**). Thus, no dissolution of C_{60} molecules was observed, and all tested C_{60}/Ti films deposited on the glass coverslips were mechanically stable in the water.

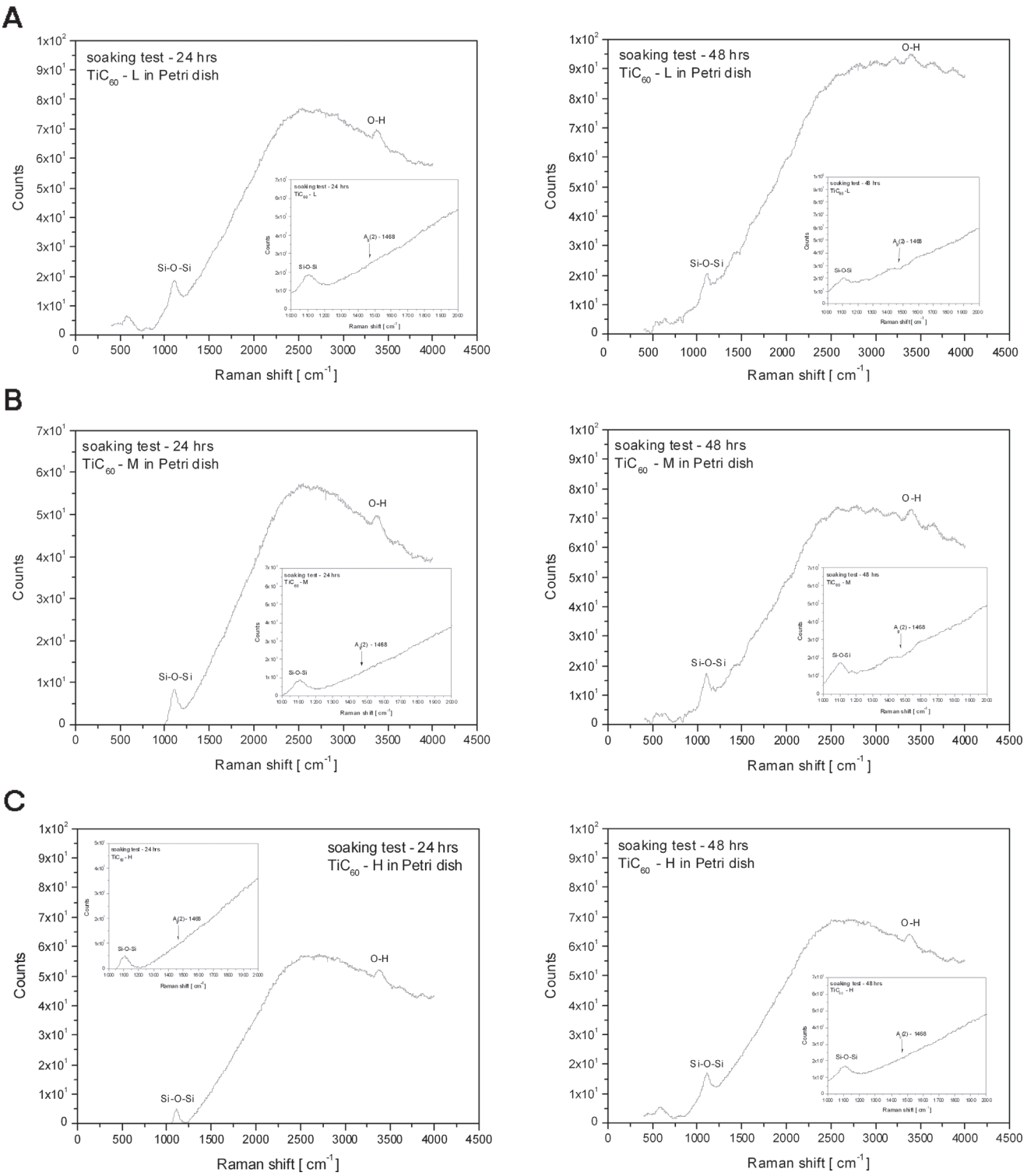

Fig 4. Raman spectrum of thin films formed in Petri dishes by evaporating water solutions after incubation of C_{60}/Ti composites with a low *(A)*, medium *(B)* and high *(C)* content of Ti for 24 hours and then for another 48 hours. No $A_g(2)$ vibration mode (i.e., no presence of C_{60}) was confirmed.

doi:10.1371/journal.pone.0123680.g004

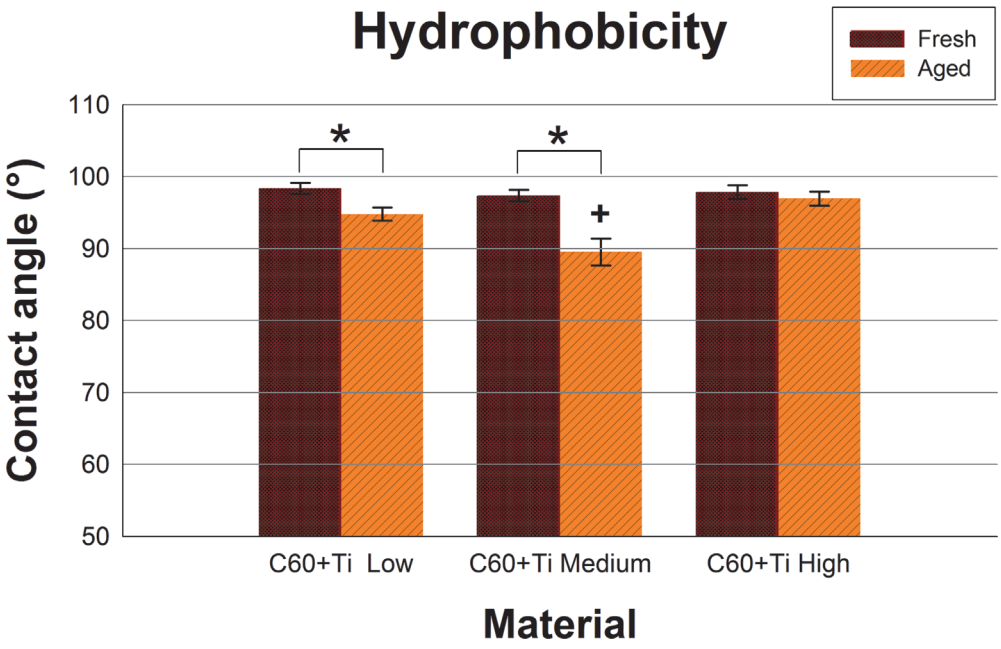

Fig 5. Static water drop contact angle of fresh and aged C_{60}/Ti composites with various Ti concentrations (low: 25%, medium: 45%, high: 70%). * significant difference between fresh and aged layers; $p \leq 0.05$.

doi:10.1371/journal.pone.0123680.g005

Hydrophobicity of C_{60}/Ti layers

Both fresh and aged layers of all C_{60}/Ti composites with various Ti concentrations were at a relatively high hydrophobic level ranging from 89.6° to 98.4°. A significant decrease in the water contact angle was observed during the aging of C_{60}/Ti films with low and medium Ti content (Fig 5, S1 Table, S1 Dataset).

This could be explained by spontaneous physicochemical changes (such as fragmentation, polymerization, oxidation and graphitization) in an air atmosphere (Fig 2; described above). This decline was not observed for aged C_{60}/Ti layers with a high Ti content (Fig 5, S1 Table, S1 Dataset), which is in correlation with the results obtained from Raman spectroscopy, where the spectra of the fresh and aged samples were very similar, and therefore fewer physicochemical changes occurred during their aging (Fig 2; described above). The presence of oxygen and the formation of oxygen-containing chemical functional groups are known to increase the surface wettability of various materials, e.g. synthetic polymers, metals or carbon-based materials (for a review see [1, 2]). In our earlier studies, oxidation and also fragmentation, polymerization and graphitization of fullerenes were observed on fullerene films exposed to 70% cold ethanol used for material sterilization.

Initial adhesion, proliferation and morphology of cells on fullerene C_{60} /Ti layers

The number of initially adhered human osteoblast-like cells MG-63 cells on day 1 after seeding on fresh (i.e., one-week-old) C_{60}/Ti composites with various Ti additions was slightly lower (the decrease correlated positively with the increase in Ti concentration) in comparison with the reference microscopic glass coverslips (Fig 6A, S2A Table, S1 Dataset); however, these reductions were not proven to be statistically significant. Similar results for cell numbers were obtained on day 3 after seeding (Fig 6B, S2B Table, S1 Dataset). The calculation of the cell

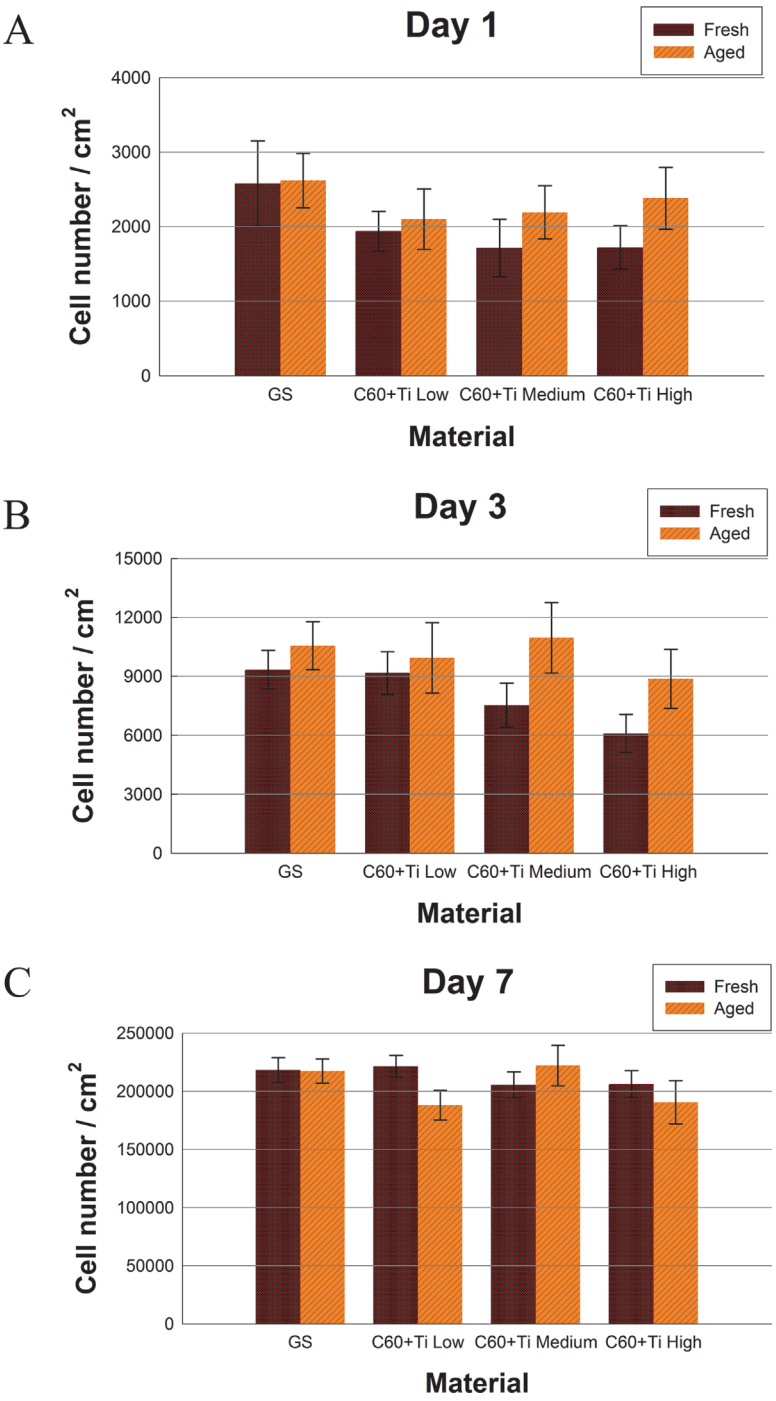

Fig 6. Numbers of human osteoblast-like MG-63 cells on fresh or aged C_{60}/Ti composites with various Ti concentrations (low: 25%, medium: 45%, high: 70%) on day 1 *(A)*, 3 *(B)* and 7 *(C)* after seeding. GS: microscopic glass coverslips, a reference material. No significant differences among the experimental groups were found.

doi:10.1371/journal.pone.0123680.g006

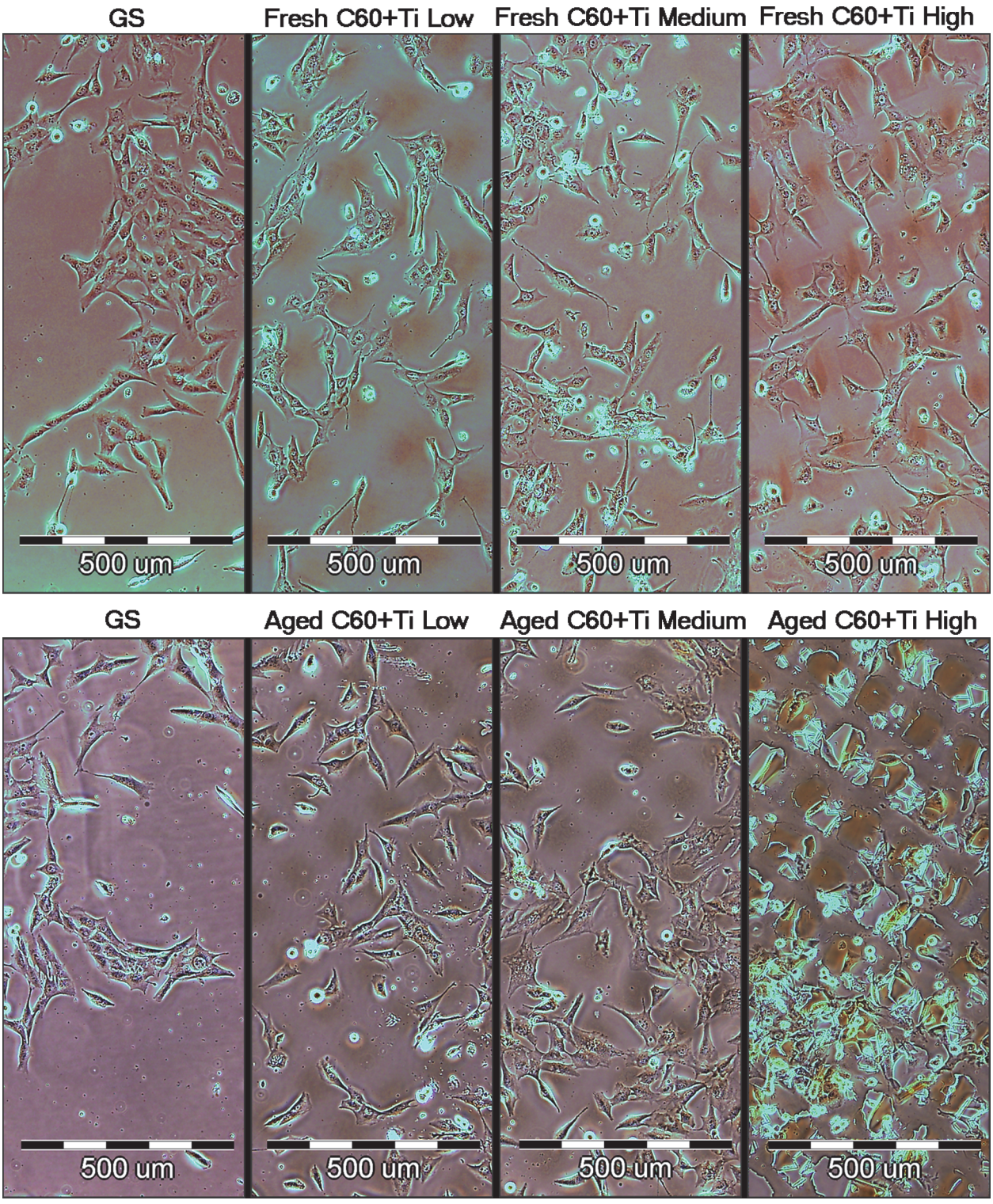

Fig 7. Morphology of human osteoblast-like MG-63 cells on day 3 after seeding on fresh and aged C_{60}/Ti composites with various concentrations of Ti (low: 25%, medium: 45%, high: 70%). GS: microscopic glass coverslips, reference material.

doi:10.1371/journal.pone.0123680.g007

population doubling time also did not reveal any significant decrease in proliferation of cells cultured on fresh C_{60}/Ti films. The doubling times of the cells cultured on all fresh samples were comparable with the reference material (**S1 and S2 Figs, S3 Table, S1 Dataset**).

On the aged C_{60}/Ti films, the initial adhesions as well as the cell numbers on all tested samples were almost the same in all culture intervals (**Fig 6, S2 Table, S1 Dataset**). The growth dynamics of cells cultured on aged composites of all Ti concentrations was also similar to that on the reference material (the doubling times are shown in **S1 and S2 Figs, S3 Table, S1 Dataset**).

In a previous study performed on pure C_{60} layers, lower numbers and slower proliferation of MG 63 cells were found on the fresh films in comparison with the control glass coverslips or with aged C_{60} films [38]. However, on aged C_{60} films, these differences diminished considerably or almost disappeared. This result was explained by changes in C_{60} molecules during their ageing, such as fragmentation, polymerization and oxidation, which decreased the reactivity of fullerenes. Interestingly, the examination of C_{60}/Ti composites in this study showed no significant differences in cell adhesion and growth between the fresh and aged films. Moreover, from this point of view, both fresh and aged layers were comparable to the reference glass coverslips. A possible explanation for this improvement of the fresh C_{60} layers for cell cultivation by co-deposition with Ti could be that fragmentation, polymerization and oxidation of C_{60} occurred during deposition of the composite films by the interaction of C_{60} molecules with Ti atoms, and not only due to the ageing of the C_{60}/Ti films. In other words, the C_{60}/Ti composites exhibited similar biocompatibility as the mix of amorphous carbon and titanium. Similarly, amorphous carbon in the form of films or electrospun nanofibrous scaffolds has been shown to provide good support for the adhesion and proliferation of mouse neuroblastoma N2a cells and rat Schwann RT4-D6P2T cells [41].

The cell morphology was similar on both fresh and aged C_{60}/Ti composites of all Ti concentrations. The cells were generally well-spread, polygonal or spindle-shaped. No cytotoxic morphological changes, such as enlarged cells or cytosolic vacuole formation, were observed on fresh or on aged C_{60}/Ti films with various Ti concentrations (**Fig 7**).

Preferential growth in grooves among the prominences was also apparent, particularly on the fresh composites (**Fig 7**). Similar cell behavior was also observed in our earlier studies performed on micropatterned pure C_{60} as well as hybrid C_{60}/Ti films [36–38, 40]. Nevertheless, on micropatterned pure C_{60} films, the preferential cell colonization in grooves was much more apparent on the fresh films than on the aged films. This was explained by the diffusion of C_{60} molecules from the prominences towards the grooves and thus lowering of the prominences during aging [38]. On the composite C_{60}/Ti films in the present study, prominences and preferential cell colonization in grooves were still apparent on the aged films, particularly those with the highest Ti concentration. This could be attributed to increased stability of the prominences due to the presence of Ti atoms.

Metabolic activity and viability of cells on fullerene C_{60} /Ti layers

In order to investigate the potential cytotoxicity of fresh and aged C_{60}/Ti composites with various Ti additions, an XTT cell proliferation assay was performed. Proportionally to the cell numbers, MG-63 cultivated for 7 days on both fresh and aged C_{60}/Ti layers showed comparable metabolic activity (i.e., activity of mitochondrial enzymes) with cells grown on control glass coverslips (**Fig 8, S4 Table, S1 Dataset**). No significant differences in metabolic activity were found among the various Ti concentrations or the ages of the C_{60}/Ti composites.

Cell viability and potential cell membrane damage were analyzed by trypan blue staining. The cells growing on all tested C_{60}/Ti composites were highly viable (over 80%) and were comparable to the cells on the reference material. No statistically significant differences in viability were observed among the various Ti concentrations or ages of the C_{60}/Ti composites (**Fig 9, S5 Table, S1 Dataset**). The improvement in metabolic activity and also in the viability of cells

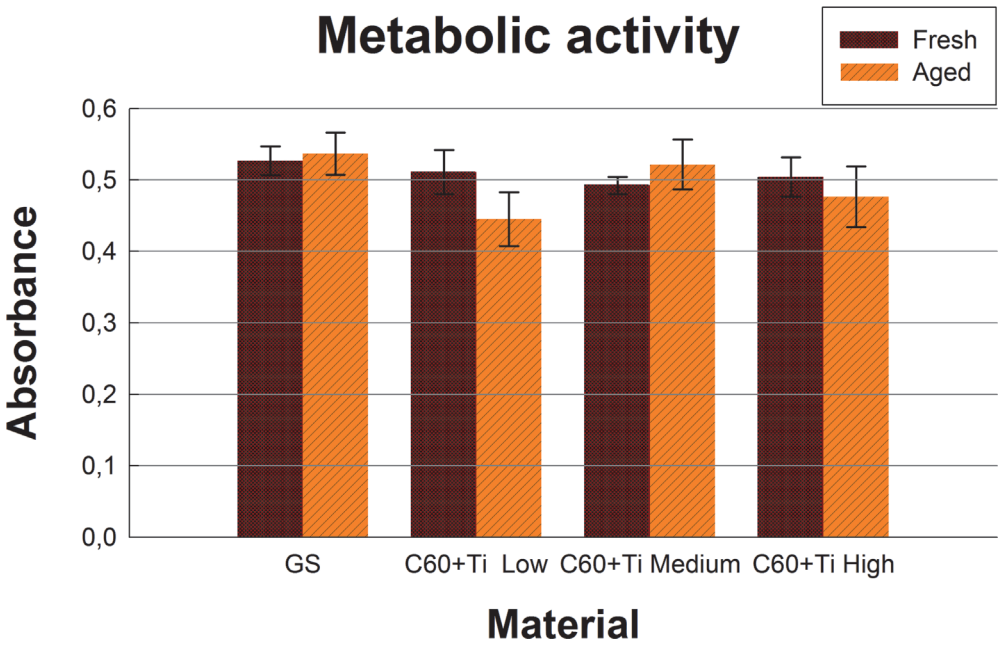

Fig 8. Metabolic activity measured by the XTT test per culture of human osteoblast-like MG-63 cells on day 7 after seeding on fresh and aged C_{60}/Ti composites with various Ti concentrations (low: 25%, medium: 45%, high: 70%). GS: microscopic glass coverslips, a reference material. No significant differences among the experimental groups were found.

doi:10.1371/journal.pone.0123680.g008

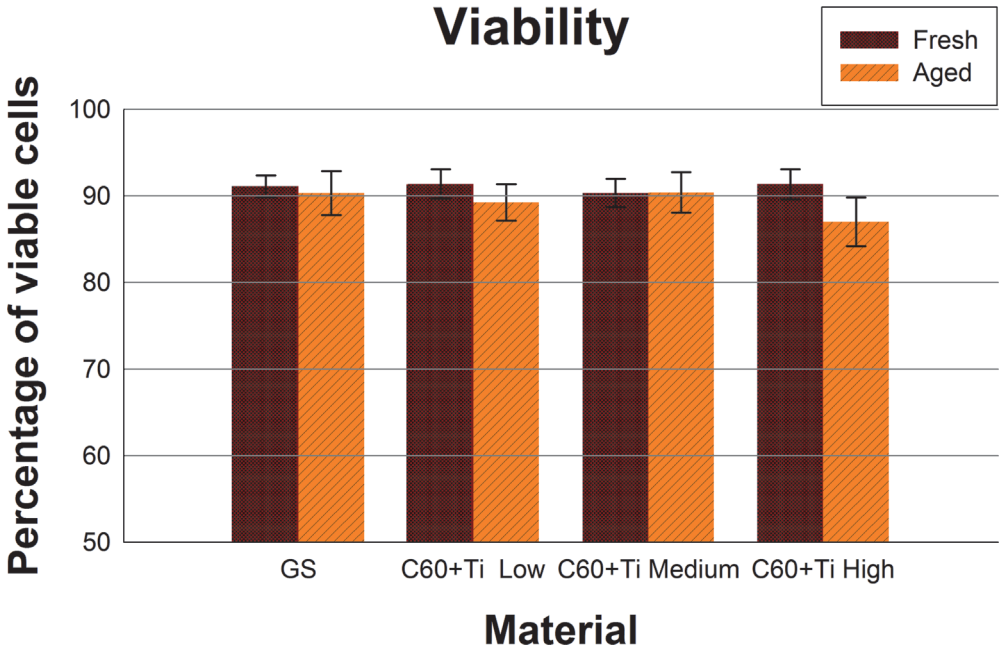

Fig 9. Viability of human osteoblast-like MG-63 cells, measured by the trypan blue exclusion test on day 7 after seeding on fresh and aged C_{60}/Ti composites with various Ti concentrations (low: 25%, medium: 45%, high: 70%). GS: microscopic glass coverslips, reference material. No significant differences among the experimental groups were found.

doi:10.1371/journal.pone.0123680.g009

A

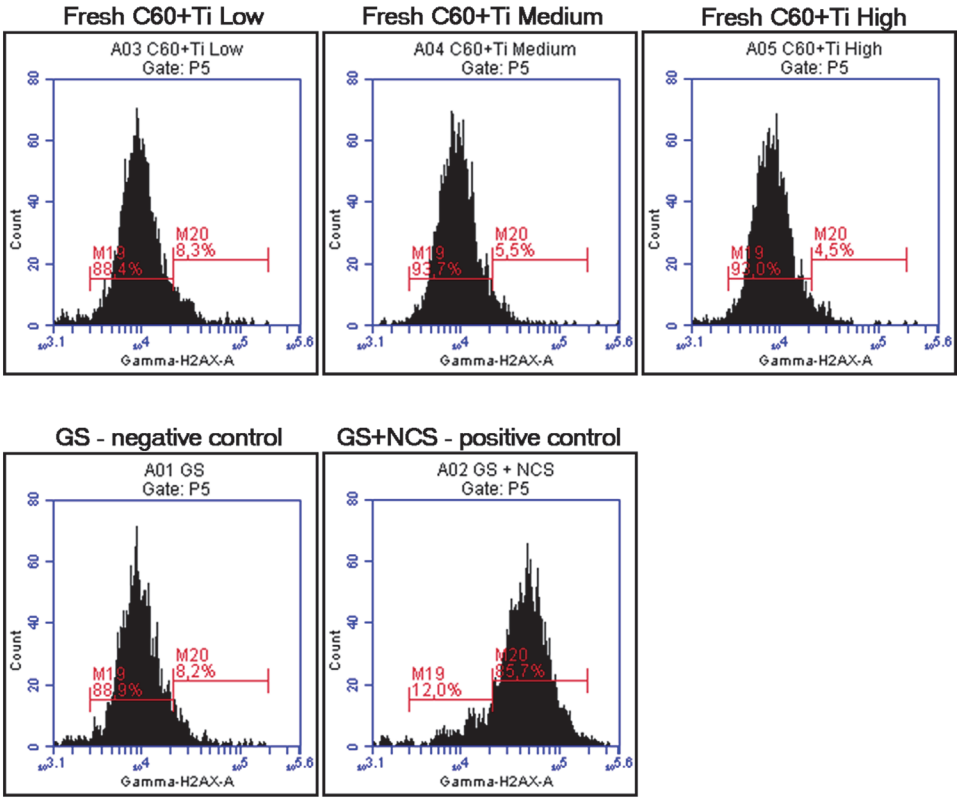
Fresh C60+Ti Low
A03 C60+Ti Low
Gate: P5
M19
88,4%
M20
8,3%
Fresh C60+Ti Medium
A04 C60+Ti Medium
Gate: P5
M19
93,7%
M20
5,5%
Fresh C60+Ti High
A05 C60+Ti High
Gate: P5
M19
93,0%
M20
4,5%
GS - negative control
A01 GS
Gate: P5
M19
88,9%
M20
8,2%
GS+NCS - positive control
A02 GS + NCS
Gate: P5
M19
12,0%
M20
85,7%
Count
Gamma-H2AX-A

B

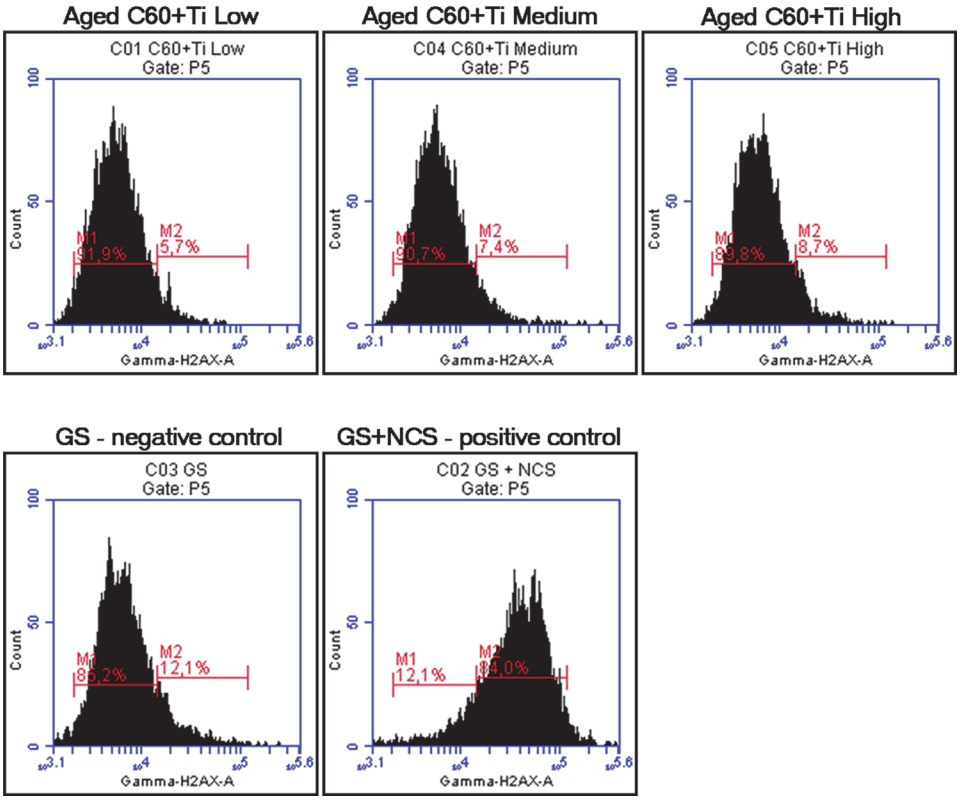
Aged C60+Ti Low
C01 C60+Ti Low
Gate: P5
M1
91,9%
M2
5,7%
Aged C60+Ti Medium
C04 C60+Ti Medium
Gate: P5
M1
90,7%
M2
7,4%
Aged C60+Ti High
C05 C60+Ti High
Gate: P5
M1
89,8%
M2
8,7%
GS - negative control
C03 GS
Gate: P5
M1
86,2%
M2
12,1%
GS+NCS - positive control
C02 GS + NCS
Gate: P5
M1
12,1%
M2
84,0%
Count
Gamma-H2AX-A

Fig 10. Flow cytometry of the marker of DNA damage response: gamma-H2AX in human osteoblast-like U-2 OS cells on fresh (A) and aged (B) C_{60}/Ti composites with various Ti concentrations (low: 25%, medium: 45%, high: 70%). GS: microscopic glass coverslips, reference material; GS+NCS: positive control to phosphorylation of histon H2AX (gamma-H2AX), induced by 1 hour incubation of U-2 OS in neocarzinostatin (NCS; 700ng/mL). M19 and M1 define the percentage of cells with no increase in DNA damage (obtained from cells growing on the reference material, GS); M20 and M2 define the percentage of cells with an increased DNA damage response represented by enhanced phosphorylation of histon H2AX (obtained from cells incubated with NCS).

doi:10.1371/journal.pone.0123680.g010

cultured on C_{60}/Ti layers (especially fresh composites) is obvious when compared to our previous study performed on pure C_{60} layers [38].

DNA damage response

It has been reported that fullerenes are able to bind directly to the minor and major grooves of double-strand DNA and to form a stable complex, which may have a negative impact on the self-repairing process of the dsDNA and may lead to a potential cytotoxic effect of fullerenes [42, 43].

We therefore studied the DNA damage response (DDR) of cells growing on fullerene films, by markers of DNA double strand breaks. For this purpose, osteosarcoma cell line U-2 OS was used instead of MG-63, which is p53-deficient. Gamma-HA2X (phosphorylated histon H2AX, a marker of early DDR) and 53BP1 (p53 binding protein), whose focal recruitment depends on a number of upstream factors, were evaluated. After 3 and 7 days of cultivation on various Ti concentrations of fresh and aged C_{60}/Ti composites, the level of gamma-H2AX phosphorylation was analyzed by flow cytometry. The results show no increase in the percentage of cells with enhanced phosphorylation of histon H2AX cultured on layers with various Ti additions in comparison to the reference glass coverslips. Moreover, there was no effect of the age of the C_{60}/Ti composites on DDR (**Fig 10**). Furthermore, the visualization of both DDR markers by immunofluorescence staining also revealed no increased recruitment or formation of either gamma-H2AX or 53BP1 foci (**Fig 11**). These results are consistent with our previous study focused on C_{60} layers [38]. In accordance with our results, fullerene C_{60} nanoparticles in suspension had no genotoxic ability in the bacterial reverse mutation assay, in the *in vitro* chromosome aberration assay, or in the *in vivo* micronucleus assay [44]. In addition, fullerenol mediated a decrease in the frequency of micronuclei and chromosome aberrations [45].

Conclusions and Further Perspectives

Our study has revealed that both fresh and aged C_{60}/Ti composites are suitable substrates for the adhesion and growth of human bone cells. However, in the case of pure fullerene C_{60} films studied earlier, aged films were better for cell colonization than fresh films, which had a certain negative impact on the cell spreading, proliferation, viability and activity of mitochondrial enzymes. Interestingly, the examination of C_{60}/Ti composites in this study showed no significant differences between fresh and aged films (caused by the improvement in the properties of the fresh layers). This difference between pure fullerene films and C_{60}/Ti composites may lie in the fact that in the composites, changes in the fullerene molecules, such as fragmentation, polymerization, oxidation and graphitization, occur not only due to aging of the material, but immediately during C_{60} and Ti co-deposition due to the interaction of C_{60} molecules and Ti atoms. In addition, studies performed on human osteoblast-like U-2 OS cells revealed no DNA damage response of these cells cultivated on fresh or aged C_{60}/Ti composites. C_{60}/Ti composites can therefore be considered as promising materials in bone tissue engineering, namely for potential coating of bone implants. The connection (association) of C_{60} with Ti may also have promising

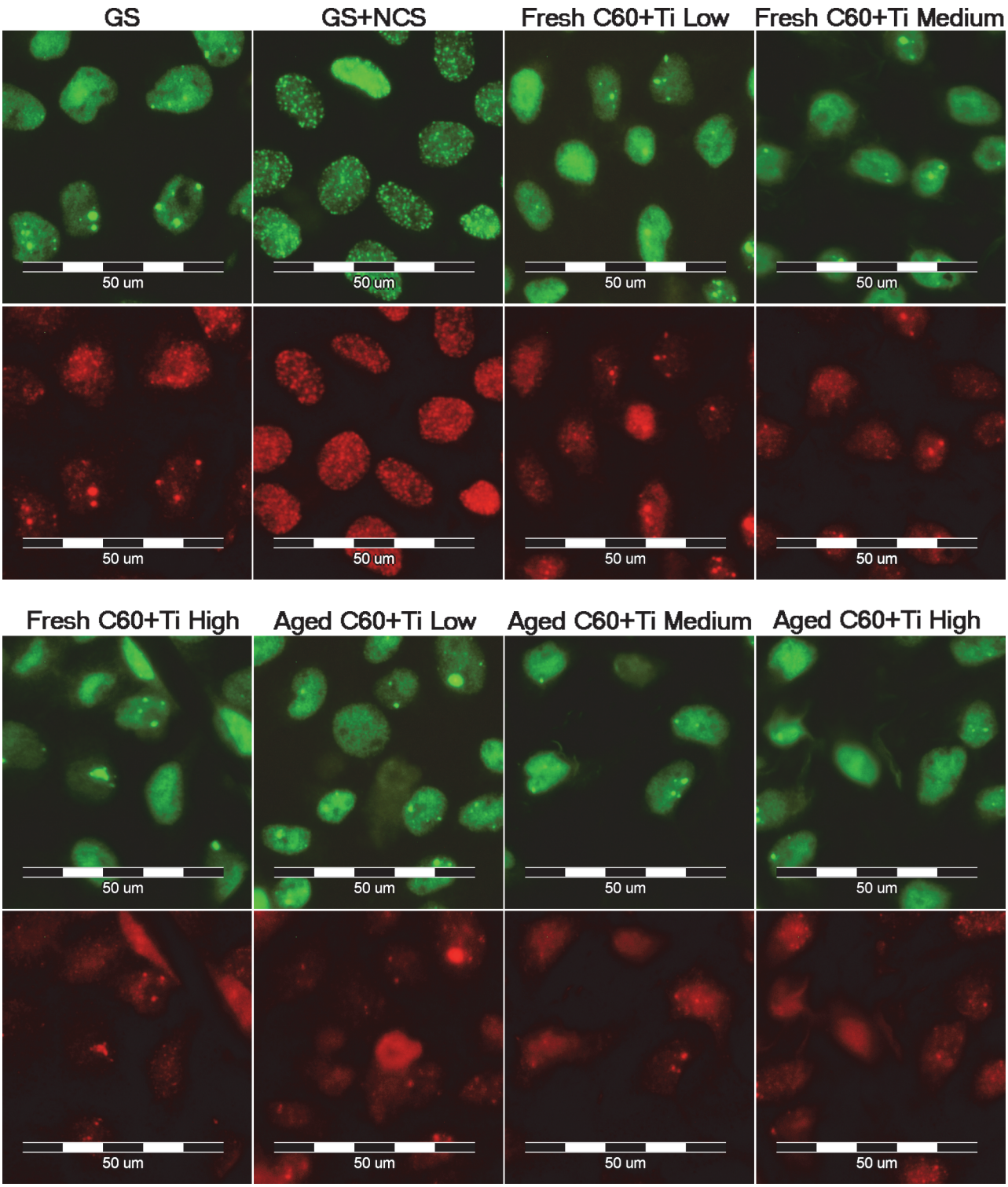

Fig 11. Immunofluorescence staining of markers of a DNA damage response: 53BP1 (green) and gamma-H2AX (red) in human osteoblast-like U-2 OS cells on fresh and aged C_{60}/Ti composites with various Ti concentrations (low: 25%, medium: 45%, high: 70%). GS: microscopic glass coverslips, reference material; GS+NCS: positive control of DNA damage response induced by 1 hour incubation of U-2 OS in neocarzinostatin (NCS; 700ng/mL).

doi:10.1371/journal.pone.0123680.g011

therapeutic potential against oxidative stress-associated conditions and in the treatment of bone and cartilage tissue destruction in arthritis.

Supporting Information

S1 Dataset. Excel sheet of raw data numbers from which the qualitative data, mean ± standard error of the mean (S.E.M) or median with interquartile range (IQR) were calculated.
(XLS)

S1 Fig. Doubling times (in hours) of human osteoblast-like MG-63 cells cultured on fresh or aged C_{60}/Ti composites with various Ti concentrations (low: 25%, medium: 45%, high: 70%). GS: microscopic glass coverslips, reference material. The data from different time intervals (day 1–3 **(A)**, day 3–7 **(B)**) is presented as median with interquartile range (IQR = Q3—Q1) obtained from 3 experiments. No significant differences among the experimental groups were found.
(TIF)

S2 Fig. Summarized doubling time (in hours) of human osteoblast-like MG-63 cells cultured on fresh or aged C_{60}/Ti composites with various Ti concentrations (low: 25%, medium: 45%, high: 70%). GS: microscopic glass coverslips, reference material. The data is presented as median with interquartile range (IQR = Q3—Q1) obtained from 3 experiments. No significant differences among the experimental groups were found.
(TIF)

S1 Table. Static water drop contact angle of fresh and aged C_{60}/Ti composites with various Ti concentrations (low: 25%, medium: 45%, high: 70%). The data is presented as mean ± standard error of the mean (S.E.M.) obtained from 10 measurements. $^{*\text{Aged}}$ significant difference between fresh and aged layers; $^{+\text{Low, High}}$ significant difference to low and high concentration of Ti among the aged samples; $p \leq 0.05$.
(DOC)

S2 Table. Numbers of human osteoblast-like MG-63 cells on fresh or aged C_{60}/Ti composites with various Ti concentrations (low: 25%, medium: 45%, high: 70%) on day 1 (A), 3 (B) and 7 (C) after seeding. The data is presented as mean ± standard error of the mean (S.E.M.) obtained from 3 experiments. GS: microscopic glass coverslips, a reference material. No significant differences among the experimental groups were found.
(DOC)

S3 Table. Doubling times (in hours) of human osteoblast-like MG-63 cells cultured on fresh or aged C_{60}/Ti composites with various Ti concentrations (low: 25%, medium: 45%, high: 70%). GS: microscopic glass coverslips, reference material. The data from different time intervals (day 1–3 **(A)**, day 3–7 **(B),** and summarized day 1–7 **(C)**) is presented as median with interquartile range (IQR = Q3—Q1) obtained from 3 experiments. No significant differences among the experimental groups were found.
(DOC)

S4 Table. Metabolic activity measured by the XTT test per culture of human osteoblast-like MG-63 cells on day 7 after seeding on fresh and aged C_{60}/Ti composites with various Ti concentrations (low: 25%, medium: 45%, high: 70%). The data is presented as mean ± standard error of the mean (S.E.M.) obtained from 3 experiments. GS: microscopic glass coverslips, a reference material. No significant differences among the experimental groups

were found.
(DOC)

S5 Table. Percentage of viable cells (human osteoblast-like MG-63 cells), measured by the trypan blue exclusion test on day 7 after seeding on fresh and aged C_{60}/Ti composites with various Ti concentrations (low: 25%, medium: 45%, high: 70%). The data is presented as mean ± standard error of the mean (S.E.M.) obtained from 3 experiments. GS: microscopic glass coverslips, reference material. No significant differences among the experimental groups were found.
(DOC)

Acknowledgments

The deposition and characterization of the C_{60}/Ti composites were carried out in the laboratories of the CANAM infrastructure (NPI ASCR Rez). Mr. Robin Healey (Czech Technical University in Prague) is gratefully acknowledged for his language revision of the manuscript.

Author Contributions

Conceived and designed the experiments: IK LB. Performed the experiments: IK VL. Analyzed the data: IK JV LB. Contributed reagents/materials/analysis tools: LB JV. Wrote the paper: IK LB JV.

References

1. Bacakova L, Grausova L, Vandrovcova M, Vacik J, Frazcek A, Blazewicz S, et al. (2008) Carbon nanoparticles as substrates for cell adhesion and growth. In: Nanoparticles: New Research (Ed. Lombardi Simone Luca), Nova Science Publishers, Inc., Hauppauge, New York, USA, pp. 39–107, ISBN 978-1-60456-704-5. doi: 10.1002/yd.272 PMID: 18855319
2. Bacakova L, Grausova L, Vacik J, Kromka A, Biederman H, Choukourov A, et al. (2011) Nanocomposite and nanostructured carbon-based films as growth substrates for bone cells. In: Advances in Diverse Industrial Applications of Nanocomposites. (Ed. Reddy Boreddy), Intech, Open Access Publisher, pp. 399–435, ISBN 978-953-307-202-9.
3. Zhang Y, Wang L, Sun Y, Zhu Y, Zhong Z, Shi J, et al. (2013) Conjugation of dexamethasone to C60 for the design of an anti-inflammatory nanomedicine with reduced cellular apoptosis. ACS Appl Mater Interfaces. 5(11): 5291–5297. doi: 10.1021/am401153k PMID: 23669026
4. Liu H, Yang X, Zhang Y, Dighe A, Li X, Cui Q (2012) Fullerol antagonizes dexamethasone-induced oxidative stress and adipogenesis while enhancing osteogenesis in a cloned bone marrow mesenchymal stem cell. J Orthop Res 30: 1051–1057. doi: 10.1002/jor.22054 PMID: 22570221
5. Yudoh K, Shishido K, Murayama H, Yano M, Matsubayashi K, Takada H, et al. (2007) Water-soluble C60 fullerene prevents degeneration of articular cartilage in osteoarthritis via down-regulation of chondrocyte catabolic activity and inhibition of cartilage degeneration during disease development. Arthritis Rheum 56: 3307–3318. PMID: 17907184
6. Yudoh K, Karasawa R, Masuko K, Kato T (2009) Water-soluble fullerene (C60) inhibits the osteoclast differentiation and bone destruction in arthritis. Int J Nanomedicine 4: 233–239. PMID: 19918370
7. Murakami M, Hyodo S, Fujikawa Y, Fujimoto T, Maeda K (2013) Photoprotective effects of inclusion complexes of fullerenes with polyvinylpyrrolidone. Photodermatol Photoimmunol Photomed 29: 196–203. doi: 10.1111/phpp.12050 PMID: 23815352
8. Møller P, Folkmann JK, Danielsen PH, Jantzen K, Loft S (2012) Oxidative stress generated damage to DNA by gastrointestinal exposure to insoluble particles. Curr Mol Med 12: 732–745. PMID: 22292440
9. Vesterdal LK, Danielsen PH, Folkmann JK, Jespersen LF, Aguilar-Pelaez K, Roursgaard M, et al. (2014) Accumulation of lipids and oxidatively damaged DNA in hepatocytes exposed to particles. Toxicol Appl Pharmacol 274: 350–360. doi: 10.1016/j.taap.2013.10.001 PMID: 24121055
10. Ferreira JL, Lonné MN, França TA, Maximilla NR, Lugokenski TH, Costa PG, et al. (2013) Co-exposure of the organic nanomaterial fullerene C60 with benzo[a]pyrene in Danio rerio (zebrafish) hepatocytes: Evidence of toxicological interactions. Aquat Toxicol 147C: 76–83.

11. Honma M, Takahashi T, Asada S, Nakagawa Y, Ikeda A, Yamakage K (2012) In vitro clastogenicity and phototoxicity of fullerene (C(60)) nanomaterials in mammalian cells. Mutat Res 749: 97–100. doi: 10.1016/j.mrgentox.2012.08.006 PMID: 22960459

12. Gao J, Wang HL, Shreve A, Iyer R (2010) Fullerene derivatives induce premature senescence: a new toxicity paradigm or novel biomedical applications. Toxicol Appl Pharmacol 244: 130–143. doi: 10.1016/j.taap.2009.12.025 PMID: 20045429

13. Rebecca M, Hsing-Lin W, Jun G, Srinivas I, Gabriel MA, Jennifer M, et al. (2009) Impact of physicochemical properties of engineered fullerenes on key biological responses. Toxicol Appl Pharmacol 234: 58–67. doi: 10.1016/j.taap.2008.08.021 PMID: 18926839

14. Rouse JG, Yang J, Barron AR, Monteiro-Riviere NA (2006) Fullerene-based amino acid nanoparticle interactions with human epidermal keratinocytes. Toxicol In Vitro 20: 1313–1320. PMID: 16759832

15. Lucafò M, Gerdol M, Pallavicini A, Pacor S, Zorzet S, Da Ros T, et al. (2013) Profiling the molecular mechanism of fullerene cytotoxicity on tumor cells by RNA-seq. Toxicology 314: 183–192. doi: 10.1016/j.tox.2013.10.001 PMID: 24125657

16. Johnston HJ, Hutchison GR, Christensen FM, Aschberger K, Stone V (2010) The biological mechanisms and physicochemical characteristics responsible for driving fullerene toxicity. Toxicol Sci 114: 162–182. doi: 10.1093/toxsci/kfp265 PMID: 19901017

17. Trpkovic A, Todorovic-Markovic B, Trajkovic V (2012) Toxicity of pristine versus functionalized fullerenes: mechanisms of cell damage and the role of oxidative stress. Arch Toxicol 86: 1809–1827. doi: 10.1007/s00204-012-0859-6 PMID: 22562437

18. Ko WB, Yun JM, Jo SW, Shon YS (2006) Ultrasonic, chemical stability and preparation of self-assembled fullerene[C60]-gold nanoparticle films. Ultrasonics. 44 Suppl 1: e363–6. PMID: 16814825

19. Harcuba P, Bacakova L, Strasky J, Bacakova M, Novotna K, Janecek M (2012) Surface treatment by electric discharge machining of Ti-6Al-4V alloy for potential application in orthopaedics. J Mech Behav Biomed Mater 7: 96–105. doi: 10.1016/j.jmbbm.2011.07.001 PMID: 22340689

20. Strasky J, Havlikova J, Bacakova L, Harcuba P, Mhaede M, Janecek M (2013) Characterization of electric discharge machining, subsequent etching and shot-peening as a surface treatment for orthopedic implants. Applied Surface Science 213: 73–78.

21. Jirka I, Vandrovcova M, Frank O, Tolde Z, Plšek J, Luxbacher T, et al. (2013) On the role of Nb-related sites of an oxidized β-TiNb alloy surface in its interaction with osteoblast-like MG-63 cells. Mater Sci Eng C Mater Biol Appl 33: 1636–1645. doi: 10.1016/j.msec.2012.12.073 PMID: 23827618

22. Vandrovcova M, Jirka I, Novotna K, Lisa V, Frank O, Kolska Z, et al. (2014) Interaction of human osteoblast-like Saos-2 and MG-63 cells with thermally oxidized surfaces of a titanium-niobium alloy. PLOS ONE 9(6): e100475. doi: 10.1371/journal.pone.0100475 PMID: 24977704

23. Vandrovcova M, Bacakova L (2011) Adhesion, growth and differentiation of osteoblasts on surface-modified materials developed for bone implants. Physiol Res 60: 403–417. PMID: 21401307

24. Bacakova L, Stary V, Kofronova O, Lisa V (2001) Polishing and coating carbon fibre-reinforced carbon composites with a carbon-titanium layer enhances adhesion and growth of osteoblast-like MG 63 cells and vascular smooth muscle cells in vitro. J Biomed Mater Res 54: 567–578. PMID: 11426603

25. Grinevich A, Bacakova L, Choukourov A, Boldyryeva H, Pihosh Y, Slavinska D, et al. (2009) Nanocomposite Ti/hydrocarbon plasma polymer films from reactive magnetron sputtering as growth support for osteoblast-like and endothelial cells. J Biomed Mat Res A 88: 952–966. doi: 10.1002/jbm.a.31918 PMID: 18384161

26. Joska L, Fojt J, Cvrcek L, Brezina V (2014) Properties of titanium-alloyed DLC layers for medical applications. Biomatter 4. pii: e29505.

27. Popa AC, Stan GE, Husanu MA, Pasuk I, Popescu ID, Popescu AC, et al. (2013) Multi-layer haemocompatible diamond-like carbon coatings obtained by combined radio frequency plasma enhanced chemical vapor deposition and magnetron sputtering. J Mater Sci Mater Med 24(12): 2695–2707. doi: 10.1007/s10856-013-5026-y PMID: 23943017

28. Tsai PC, Chiang JY, Hwang YF (2008) Characteristics and mechanical properties of titanium-containing diamond like carbon films deposited by cathodic arc evaporation. J Nanosci Nanotechnol 8(5): 2516–2521. PMID: 18572676

29. Dwivedi N, Kumar S, Malik HK (2011) Nanostructured titanium/diamond-like carbon multilayer films: deposition, characterization, and applications. ACS Appl Mater Interfaces 3(11): 4268–4278. doi: 10.1021/am200939j PMID: 21942626

30. Talyzin AV, Jansson U (2003) A comparative Raman study of some transition metal fullerides. Thin Solid Films 429(1–2): 96–101.

31. Vacik J, Naramoto H, Narumi K, Yamamoto S, Abe H (2004) Study of the nickel-fullerene nano-structured thin films. Nucl Instrum Meth B 219–220: 862–866.

32. Vacik J, Lavrentiev V, Hnatowicz V, Yamamoto S, Vorlicek V, Stadler H (2009) Spontaneous partitioning of the Ni+C60 thin film grown at RT. J Alloy Compd 483: 374–377.

33. Vacik J, Lavrentiev V, Vorlicek V, Bacakova L, Narumi K (2010) Effect of ion irradiation on structure and thermal evolution of the Ni–C60 hybrid systems. Nucl Instr Meth Phys Res B 268(11–12): 1976–1979.

34. Vacik J, Lavrentiev V, Horak P, Michalcova A, Abe H (2011) Spontaneous growth of the polyhedral fullerene crystals in the supersaturated Ni-C60 composite. J Alloy Compd 509S: S380–S383.

35. Liu X, Jia Y, Guo L, Wang G (2005) Photoelectric investigations of charge-transferring metal-doped [60] fullerenes. Solar Energy Materials and Solar Cells 87(1–4): 5–10.

36. Vandrovcova M, Vacik J, Svorcik V, Slepicka P, Kasalkova N, Vorlicek V, et al. (2008) Fullerene C60 and hybrid C60/Ti films as substrates for adhesion and growth of bone cells. Phys. Status Solidi A 205: 2252–2261.

37. Vacik J, Lavrentiev V, Novotna K, Bacakova L, Lisa V, Vorlicek V, et al. (2010) Fullerene (C60)–transitional metal (Ti) composites: Structural and biological properties of the thin films. Diam Related Mater 19: 242–246.

38. Kopova I, Bacakova L, Lavrentiev V, Vacik J (2013) Growth and potential damage of human bone-derived cells on fresh and aged fullerene C_{60} films. Int J Mol Sci 14: 9182–9204. doi: 10.3390/ijms14059182 PMID: 23624607

39. Dresselhaus MS, Dresselhaus G, Eklund PC (1996) Science of fullerenes and carbon nanotubes, Academic Press, San Diego, CA, ISBN 012-221820-5.

40. Grausova L, Vacik J, Bilkova P, Vorlicek V, Svorcik V, Soukup D, et al. (2008) Regionally-selective adhesion and growth of human osteoblast-like MG 63 cells on micropatterned fullerene C(60) layers. J Optoelectronics Adv Mater 10: 2071–2076.

41. Jain S, Sharma A, Basu B (2013) In vitro cytocompatibility assessment of amorphous carbon structures using neuroblastoma and Schwann cells. J Biomed Mater Res B Appl Biomater 101: 520–531. doi: 10.1002/jbm.b.32852 PMID: 23359403

42. Zhao X, Striolo A, Cummings PT (2005) C_{60} binds to and deforms nucleotides. Biophys J, 89: 3856–3862. PMID: 16183879

43. Xu X, Wang X, Li Y, Wang Y, Yang L (2012) A large-scale association study for nanoparticle C_{60} uncovers mechanisms of nanotoxicity disrupting the native conformations of DNA/RNA. Nucleic Acids Res 40: 7622–7632. doi: 10.1093/nar/gks517 PMID: 22661584

44. Shinohara N, Matsumoto K, Endoh S, Maru J, Nakanishi J (2009) In vitro and in vivo genotoxicity tests on fullerene C60 nanoparticles. Toxicol Lett 191(2–3): 289–296.

45. Mrdanović J, Solajić S, Bogdanović V, Stankov K, Bogdanović G, Djordjevic A (2009) Effects of fullerenol C60(OH)24 on the frequency of micronuclei and chromosome aberrations in CHO-K1 cells. Mutat Res 680: 25–30. doi: 10.1016/j.mrgentox.2009.08.008 PMID: 19733687